



1 An improved high-resolution passenger vehicle emission 2 inventory for China using ride-hailing big data

3 Baojie Li ¹, Zhihui Shen ¹, Yan Li ², Yongqi Zhao ³, Wanglijing Gu ¹, Junjie Liu ¹, Yun
4 Kai Yang ¹, Weimeng Zhang ¹, Ziqian Ma ¹, Hong Liao ¹

5 ¹Collaborative Innovation Center of Atmospheric Environment and Equipment Technology, Jiangsu Key
6 Laboratory of Atmospheric Environment Monitoring and Pollution Control, School of Environmental
7 Science and Engineering, Nanjing University of Information Science & Technology, Nanjing 210044,
8 China

9 ²School of Urban Planning and Design, Peking University Shenzhen Graduate School, Shenzhen 518055,
10 China

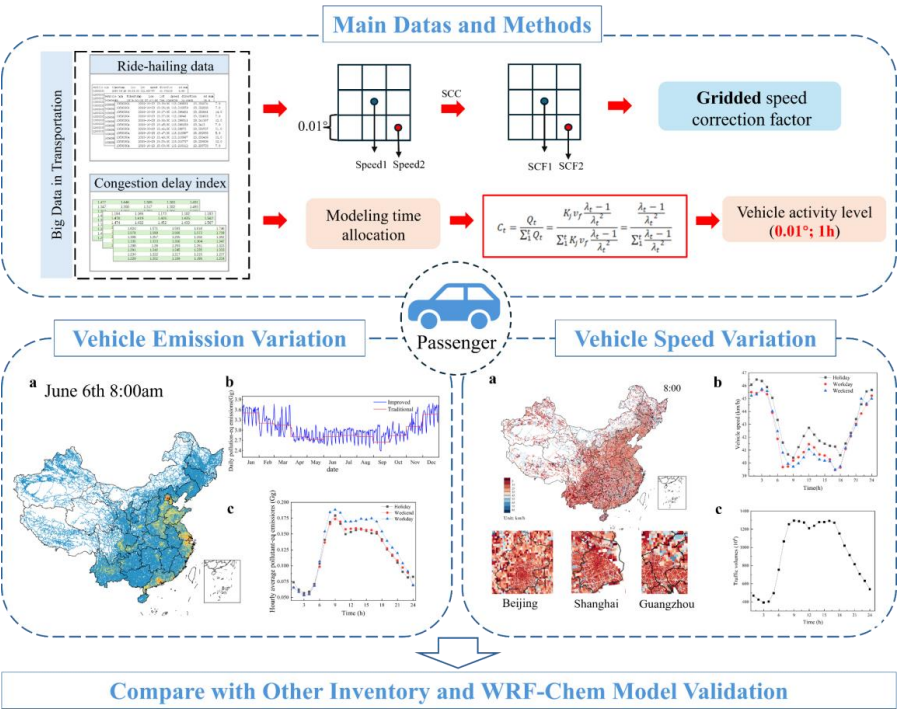
11 ³Institute of Atmospheric Physics, Chinese Academy of Sciences, Beijing 100029, China

12 *Correspondence to:* Baojie Li (baojieli@nuist.edu.cn)

13 Hong Liao (hongliao@nuist.edu.cn)

14

15 **ABSTRACT:** As the global automotive industry continues to grow rapidly, the increasing number of
16 passenger vehicles has contributed to worsening air pollution. However, previous studies have
17 insufficiently addressed nationwide hourly vehicle emissions. This study firstly utilized big data of ride-
18 hailing services and traffic flow model to obtain nationwide hourly gridded speed and traffic volume.
19 Then we established a high spatiotemporal resolution ($0.01^\circ \times 0.01^\circ$; 1h) emission inventory by using
20 multiple correction factors. The annual amount of CO, VOCs, NO_x, PM and NH₃ emitted from national
21 passenger vehicles in 2019 were 4087.8, 1069.4, 211.7, 1.9, 77.5 kt, respectively. Despite occupying
22 merely 0.8% of the national territory, urban areas generated 35.3% of the country's total vehicle
23 emissions, due to high local traffic volumes and relatively low vehicle speeds. From a temporal
24 perspective, passenger vehicle emissions exhibit significant holiday effect and weekend effect. In
25 addition, hourly average emissions on workday exceeded those of weekend and holiday by 8 % and 5 %
26 during the morning peak, with these differences increasing to 12% and 18% during the evening peak.
27 Current traditional emission methodology might underestimate emissions by 31.5%. We also used the
28 WRF-Chem model for simulation validation. This hourly-scale inventory provides quantitative support
29 for the precise implementation of pollution control and early warning.



30

31

Graphical abstract

32

1. Introduction

33

34

35

36

37

38

39

40

41

42

43

The number of vehicles in China grew from 14.53 million to 260 million over the past two decades, with an average annual growth rate of 16.39%(MEE, 2020a). This growth has driven economic development while adversely impacting air quality and human health(Anenberg et al., 2017). Premature deaths attributable to PM_{2.5} in China amounted to 1.33 million in the year 2020, of which motor vehicle emissions contributed approximately 12.5%(Li et al., 2023b; Luo et al., 2022). In 2019, passenger vehicles accounted for about 80% of the total vehicle population in China (NBS, 2020b) and contributed significantly to vehicular emissions (e.g., VOCs accounted for more than 50% of the total)(Li et al., 2023a). Quantification of passenger vehicle emission characteristics is imperative for the evaluation of relevant emission reduction policies.

With the advancement of regional air quality simulation technology and the increasing demand for atmospheric environmental management, traditional traffic emission statistical methods have become



44 inadequate to meet current refined management requirements(Gao et al., 2020). To address this issue,
 45 previous studies have developed numerous methods for constructing refined vehicle emission inventories.
 46 The first category involves constructing high spatiotemporal resolution traffic emission inventories by
 47 using complex emission models, such as COPERT, MOVES, and IVE(Yang et al., 2018; Yu et al., 2021;
 48 Wen et al., 2020; Huo et al., 2009). The second category utilizes big data on transportation. For instance,
 49 Daniela et al.(Dias et al., 2018) improved the characterization of the spatial variation of vehicle speeds
 50 at the city scale through GPS modeling, and Deng et al.(Deng et al., 2020) utilized the BeiDou Navigation
 51 Satellite System (BDS) to establish an emission inventory with lower uncertainty for the Beijing-Tianjin-
 52 Hebei (BTH) region. However, due to the difficulties in obtaining large-scale and long-term traffic data,
 53 most studies are also limited to cities or urban agglomerations, such as Chengdu, Beijing, and the Pearl
 54 River Delta (PRD) (Li et al., 2020b; Zheng et al., 2009; Wen et al., 2022), for emission calculations.
 55 There is a lack of hourly-resolution emission estimates at the national level.

56 Emission factors are generally considered to be one of the primary sources of uncertainty in
 57 emission inventories(Charis et al., 2010). Many scholars focus merely on the impact of vehicle
 58 technology improvements, fuel types, and vehicle aging on emission factors, while often neglecting the
 59 influence of speed(Xu et al., 2021; Andrew et al., 2003). Speed has the greater impact on emission factors
 60 compared to other correction factors, as it fluctuates dynamically within the same region, while other
 61 correction factors remain relatively constant over time. This difference is primarily attributed to
 62 variations in engine workload and combustion efficiency at different speeds(Sun et al., 2020; Andrew et
 63 al., 2003). The impact of speed on vehicle emissions is both significant and complex. For NO_x, the
 64 emission rate of light-duty passenger vehicles at high speeds (>50 km h⁻¹) is 1.6 times that at low speeds
 65 (10-20 km h⁻¹), while the emission rates of HC and CO at low speeds are 1.6 times and 2.3 times that of
 66 high-speed driving, respectively(Guo et al., 2020). Given this impact, accurate calculation of speed
 67 correction factors is important for reducing the uncertainty of emissions factors.

68 The temporal allocation method can also directly affect the accuracy of high-resolution emission
 69 inventories. Previous studies have established emission inventories at monthly scales(Zheng et al., 2014;
 70 Jiang et al., 2020; Zhou et al., 2016), or roughly obtained daily-scale data, followed by the construction
 71 of a regional-level hourly-scale inventory, such as Biswal et al.(Akash et al., 2022) who systematically
 72 analyzed hourly gridded road traffic emissions in Delhi city and Sun et al.(Sun et al., 2021) who
 73 considered the influence of the vehicle age-annual average mileage curve and estimated hourly emission



on a $0.01^\circ \times 0.01^\circ$ grid in Tianjin. However, they have ignored the fluctuations in daily emissions caused by workday, weekend, and holiday, which has significant uncertainty.

To address these gaps, this study aims to improve the accuracy of emission estimations by utilizing big data of ride-hailing services to obtain nationwide speed distribution on a 0.01° grid for the first time and apply it to the speed correction of emission factors. We construct a high spatiotemporal resolution ($0.01^\circ \times 0.01^\circ$; 1h) emission inventory of atmospheric pollutants from passenger vehicles in China in 2019 by further integrating traffic flow models and big data of the congestion delay index. The study also explores the spatiotemporal characteristics of pollutant emissions from passenger vehicles, compares the results with traditional calculation methods, and further evaluates the inventory improvement using WRF-Chem model.

2. Data and methodology

2.1. Estimation of emission inventories

The emission inventory for each pollutant (CO, VOCs, NO_x, PM, NH₃) for passenger cars was estimated with the following equation:

$$E_j = \sum_{i,p,k,t} V_{p,i,k,t} \times BEF_{p,j} \times \varphi_{p,i,j,t} \times \gamma_{p,i,t} \times \lambda_{p,j} \times \theta_{p,j} \times 10^{-9} \quad (1)$$

$$V_{p,i,k,t} = VP_{p,i,k,t} \times VKT_{p,i,t} \quad (2)$$

$$TPE_s = \sum_j \frac{E_j}{PEV_j} \quad (3)$$

In Eq.(1) and Eq.(2), E represents pollutant emissions, t; i represents the grid; j represents the pollutant type, including CO, PM, VOCs, NO_x and NH₃; k represents the vehicle type, including small passenger cars and mini passenger cars; p represents the province; VP, VKT, and BEF represent the vehicle population, annual average vehicle kilometers traveled and baseline emission factors, with units of vehicles, km per year, and g km⁻¹, respectively. φ is the environmental correction factor (including temperature correction factor, humidity correction factor, and altitude correction factor); γ is the speed correction factor; λ is the deterioration correction factor; θ represents other correction factors (including sulfur content correction factor and ethanol blending correction factor). In Eq.(3), TPEs represents the total pollutant equivalents (For assessing the extent of environmental and techno-economic hazards posed by various pollutants), and PEV represents the pollutant equivalent value(MEE, 2018). This study adopted the VKT values for LDPVs in 2019 from the research of Ma et al.(Ma et al., 2022). By utilizing



102 data from the China Statistical Yearbook from 2004 to 2019, the lifetime curve of passenger vehicles
 103 was obtained, which further yielded the proportion and total amount of passenger vehicles under each
 104 emission standard in each province in 2019 (Figure S1). The baseline emission factors were obtained
 105 based on other literature (Wen et al., 2023; MEE, 2014; EEA, 2019), with specific details provided in
 106 Table.S1.

107 **2.2. Quantification of high-resolution emission factors based on big data of ride-hailing**

108 **2.2.1 Gridded speeds and determination of their correction factors**

109 A total of 23.6 billion vehicle trajectory data were collected in this study from Amap Ride-hailing
 110 Platform(https://dache.amap.com/amap_mini#/), including workdays (September 24th, October 23rd),
 111 weekends (September 28th, October 26th) and holidays (September 13th, October 1st) (Table S2). Based
 112 on the vehicle speed data from these days, we assumed that the vehicle speeds on other dates did not vary
 113 significantly compared to these representative days. Each vehicle sent data every 3 seconds. Using
 114 Python, we processed the data to obtain hourly resolution vehicle speeds on a 0.01° grid. Finally, we
 115 obtained gridded hourly vehicle speeds for three representative days: workdays, weekends, and holidays.

116 Furthermore, we adopted the improved speed correction curve (SCC) method proposed by Sun et
 117 al.(Sun et al., 2020) to obtain continuous speed correction factor values for VOC, NO_x, and CO,
 118 ultimately resulting in gridded speed correction factors. For specific SCC of various pollutants, please
 119 refer to Table.S3.

120 **2.2.2 Corrections for other emission factors**

121 In the equations, ϕ utilizes daily temperature, humidity, and elevation data, all obtained from ERA5
 122 (<https://cds.climate.copernicus.eu/datasets>). The deterioration correction factor λ is calculated using
 123 relevant equations and coefficients from the EEA.(2019) θ includes the sulfur content correction factor
 124 and the ethanol blending correction factor, which are based on the corresponding values from GEI(MEE,
 125 2014). Specific values can be found in Table.S4.

126 **2.3. High-resolution vehicle activity level data combined with traffic flow models**

127 For time allocation for vehicle activity levels, the following formula can be used:

$$128 \quad V_{p,t,k} = C_{p,t} \times V_{p,k} = C_{p,t} \times VP_{p,k} \times VKT \quad (4)$$

129 where $V_{p,t,k}$ is the vehicle activity level of model k in province p in time period t ; $V_{p,k}$ is the number



130 of vehicles of model k in province p.

131 $C_{p,t}$ is the time allocation coefficient of province p at time period t. It is obtained by combining the
 132 congestion delay index obtained from Baidu Map Traffic and Travel Big Data Platform
 133 (<https://jiaotong.baidu.com/>) with the three-parameter model of traffic flow(Jinping et al., 2024), which
 134 is constructed as follows:

135 The congestion delay index is defined as the ratio of the actual time spent by residents on one trip
 136 to the time spent in a smooth state when the travelling distance is the same, and its calculation formula
 137 is:

$$138 \quad \lambda = \frac{T}{T_f} = \frac{\frac{L}{v}}{\frac{L}{v_f}} = \frac{v_f}{v} \quad (5)$$

139 Where, λ is the congestion delay index; T is the actual time spent travelling; T_f is the time spent
 140 travelling at the smooth speed; L is the length of the road section, v is the actual travelling speed, and v_f
 141 is the smooth speed of the vehicle, then:

$$142 \quad v = \frac{v_f}{\lambda} \quad (6)$$

143 Combined with the basic three-parameter model of traffic flow, the relationship between flow rate
 144 and congestion index can be derived:

$$145 \quad Q = K_j \left(v - \frac{v^2}{v_f} \right) = K_j \left[\frac{v_f}{\lambda} - \frac{\left(\frac{v_f}{\lambda} \right)^2}{v_f} \right] = K_j v_f \frac{\lambda - 1}{\lambda^2} \quad (7)$$

146 Where Q is the flow rate; λ is the congestion delay index; K_j is the congestion density; v_f is the
 147 unimpeded vehicle speed, and K_j and v_f are constants.

148 In turn, we obtain the formula for calculating the time allocation coefficient of motor vehicle
 149 emissions:

$$150 \quad C_t = \frac{Q_t}{\sum_1^t Q_t} = \frac{K_j v_f \frac{\lambda_t - 1}{\lambda_t^2}}{\sum_1^t K_j v_f \frac{\lambda_t - 1}{\lambda_t^2}} = \frac{\lambda_t - 1}{\lambda_t^2} \quad (8)$$

151 Where C_t is the motor vehicle emission time allocation coefficient; t is time; and Q_t denotes the
 152 volume of traffic in time period t.

153 Regarding the spatial allocation of the vehicle activity level, this study was done using the road
 154 length data provided by Golder Maps as an allocation index(Gómez et al., 2018), and the gridded vehicle
 155 activity level at $0.01^\circ \times 0.01^\circ$ resolution was calculated according to the following formula:



$$V_{p,i,k,t} = \frac{L_{p,i}}{\sum_i L_{p,i}} \times V_{p,t,k} \quad (9)$$

where $V_{p,i,k,t}$ is the activity level of model k in the i grid of province p in time period t ; $V_{p,t,k}$ is the number of vehicles of model k in province p in time period t ; and $L_{p,i}$ is the length of the road in the i grid of province p .

2.4 WRF-Chem model setting

To verify the superiority of the improved inventory, this study employed the WRF-Chem model to simulate the atmospheric concentrations of $PM_{2.5}$ and O_3 in the Jiangsu and Shanghai regions (longitude range: $117.5^\circ E \sim 122.0^\circ E$; latitude range: $30.0^\circ N \sim 35.10^\circ N$) from February 1, 2019 to February 18, 2019 (covering the Spring Festival period and the subsequent week). A two-layer nested model with spatial resolutions of 9×9 km and 3×3 km, respectively, was adopted for the simulation. The specific simulated region is illustrated in Figure S2(a).

The inventory developed in this study was used as the input data for traffic sources, while data from the ABaCAS database was adopted for other emission sources; these two sets of data were jointly utilized to generate the anthropogenic emission files required for the WRF-Chem model (Li et al., 2023a). The $1^\circ \times 1^\circ$ Final Operational Global Analysis (FNL) data provided by the National Centers for Environmental Prediction (NCEP, <https://rda.ucar.edu/datasets/ds083.2/>) was used to obtain the initial meteorological conditions and boundary conditions. Real-time biomass burning emissions were derived from the Fire Inventory from NCAR (FINN, <https://www2.aocom.ucar.edu/modeling/finn-fire-inventory-ncar>). The global simulation results from CAM-Chem (<https://www.aocom.ucar.edu/cam-chem/cam-chem.shtml>) were employed as the initial chemical conditions and boundary conditions. The specific parameterization schemes are presented in Table S5.

This study used observational data from national monitoring stations within the study area to evaluate the simulation results of the emission inventory developed in this study and the traditional inventory, as well as the improvement effects at stations in the top 20% by road density. The simulation results were verified by calculating the normalized mean deviation (NMB) and Correlation Coefficient (R).



182 3. Results and discussion

183 3.1. Spatiotemporal variation of vehicle speed and traffic flow

184 Vehicle speed and traffic volume are important parameters for describing vehicle driving conditions
 185 and traffic flow characteristics. The nationwide average passenger vehicle speed was 42.42 km h^{-1} . The
 186 high concentration of work and business activities in the eastern China during the daytime, combined
 187 with its large vehicle population, led to generally slower vehicle speeds at 8:00 compared to 22:00.
 188 Especially in the key cities such as Beijing, Shanghai, and Guangzhou, city vehicle speeds at 8:00 a.m.
 189 typically were $36.4 \pm 0.3 \text{ km h}^{-1}$ due to significantly increased traffic flow during the morning peak and
 190 the circular radial road network which might concentrate traffic flow (Liu et al., 2018). Specific to the
 191 road, the average driving speeds were higher on national highways (8:00: 67.12 km h^{-1} ; 22:00: 68.59 km
 192 h^{-1}), national roads (8:00: 40.05 km h^{-1} ; 22:00: 42.92 km h^{-1}), and provincial roads (8:00: 38.18 km h^{-1} ;
 193 22:00: 41.46 km h^{-1}) compared to other types of roads (Fig. 1a and Fig. 1b). During the off-peak period at
 194 22:00, differences in traffic flow speeds across various road types were more apparent. The vehicle
 195 speeds on some provincial and county roads had increased significantly. This reflected the non-
 196 uniformity of traffic flow distribution (Guan et al., 2024).

197 There were also differences in average vehicle speeds between provinces, with Inner Mongolia,
 198 Jiangxi, and Qinghai having higher speeds (Fig. 1c). While Yunnan Province had the lowest average
 199 vehicle speed, which might be related to its unique topography. Approximately 94% of Yunnan Province
 200 was mountainous, with an average elevation exceeding 2,000 meters (Zhijia et al., 2016). These complex
 201 topographical conditions influenced the actual driving speed of vehicles (Hou et al., 2019). In addition,
 202 compared to the Northeast China (NE: 8:00: 44.18 km h^{-1} ; 22:00: 48.37 km h^{-1}), the average vehicle
 203 speeds in the Northwest China (NW: 8:00: 36.89 km h^{-1} ; 22:00: 40.41 km h^{-1}), the East China (EC:
 204 8:00: 39.89 km h^{-1} ; 22:00: 44.56 km h^{-1}), and the South China (SC: 8:00: 40.45 km h^{-1} ; 22:00: 44.16 km
 205 h^{-1}) regions were lower, due to the NE was predominantly characterized by plains, and its population and
 206 transportation network were not as dense as those in the CC and SC (Fig. 1c) (Xu et al., 2023).

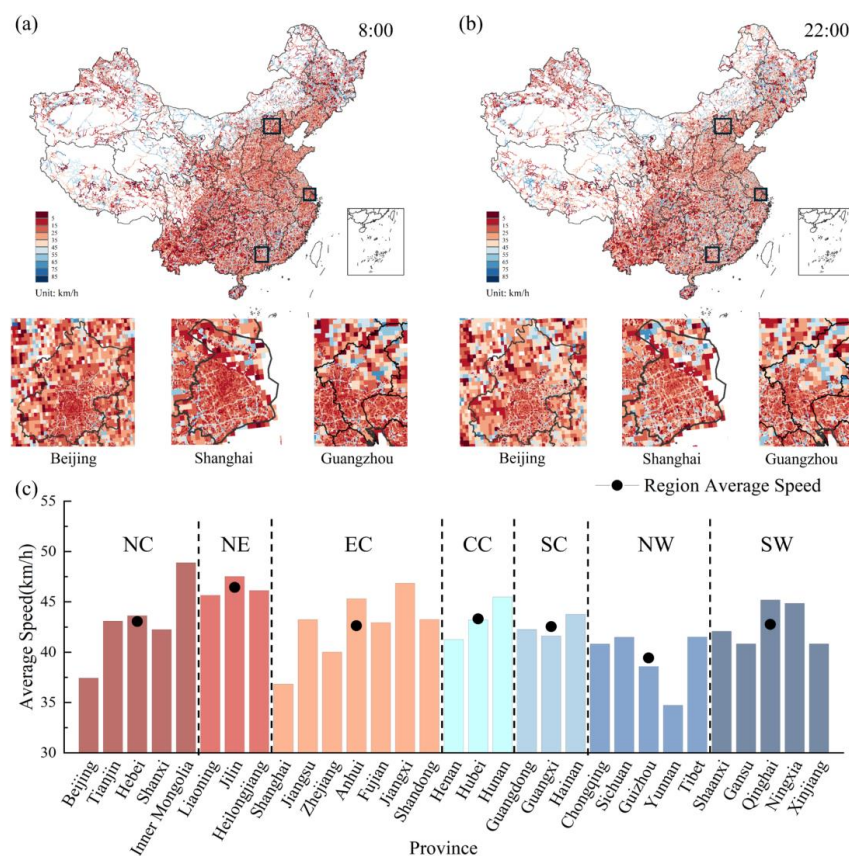
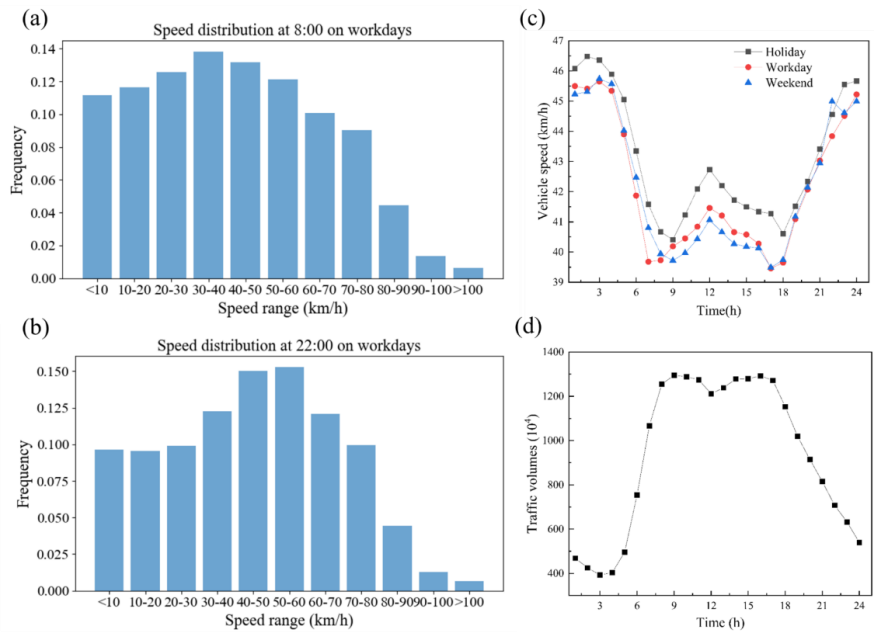


Figure 1. Average speed in China: Spatial distribution of speeds on a 0.01° grid at (a) 8:00 and (b) 22:00 ; (c) Average speeds of provinces and regions, where NC: North China; NE: Northeast China; EC: East China; CC: Central China; SC: South China; NW: Northwest China; SW: Southwest China.

Based on ride-hailing big data, the average speed of passenger vehicles fluctuated across different times. The daily average traffic speeds on workday and weekend were consistent, with both lower than on holiday, at 42.108, 42.111, and 43.032 km h⁻¹, respectively. The higher holiday speed (Fig.2c) can be attributed to reduced urban congestion resulting from increased public transportation use for leisure travel on holidays(Zhang and Gao, 2023b). All three-day types exhibited two low-speed valleys from 7:00-9:00 and 17:00-19:00, with the workday morning valley occurring one hour earlier compared to weekend, consistent with findings by Yang et al.(Yang et al., 2017). The national average speed frequency distribution differed at 8:00 and 22:00 on workday (Fig.2a and Fig.2b), primarily concentrated at 22.07±0.2 km h⁻¹ and 44.59±0.3 km h⁻¹, respectively. The large difference in speed between these two



220 periods is due to the variation in traffic volumes, as illustrated by the inverse relationship between hourly
221 traffic volume and speed distribution (Fig.2d).



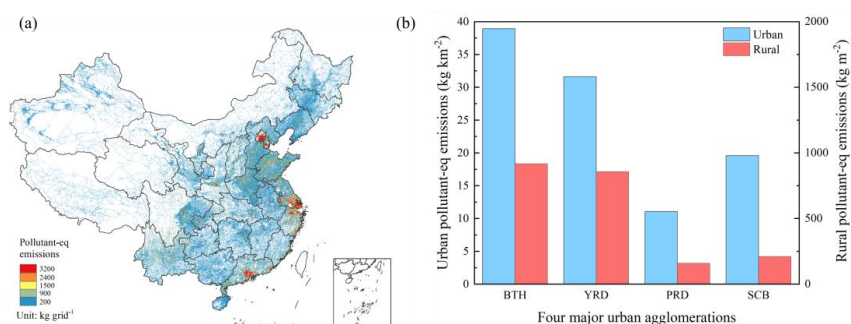
222
223 **Figure 2. Characteristics of speed and traffic volume changes: speed distribution at (a) 8:00 and (b) 22:00 on**
224 **workdays; (c) Hourly speed variation on weekend, workday and holiday and (d) hourly traffic volume**
225 **variation.**

226 3.2. Total passenger vehicle emissions in 2019

227 The annual amount of CO, VOCs, NO_x, PM and NH₃ emitted from national passenger vehicles in
228 2019 were 4087.8, 1069.4, 211.7, 1.9, 77.5 kt, respectively and TPEs was 1.6×10^3 kt. Considering these
229 pollutants exhibited similar emission patterns, this study focused on analyzing the total pollutant
230 equivalent emissions. Pollutant emissions from passenger vehicles showed significant spatial
231 heterogeneity. Urban areas, despite occupying only 0.8% of the country's total land area, accounted for
232 a high 35.3% of total vehicle emissions. High-pollution areas mainly concentrated in four urban
233 agglomerations (BTH、YRD、PRD、SCB) (Fig.3a). These areas were densely populated with high
234 vehicle usage frequency, contributing significantly to the total emissions at 48.54%. Specific emissions
235 by province are shown in Table S6. The urban emission density of vehicles within four urban
236 agglomerations was significantly higher compared to rural areas (Fig.3b), as most passenger vehicles
237 primarily operated in urban(Loder et al., 2019).



238 This study conducted a comparative analysis of the results from different studies to verify the
 239 accuracy of the emission inventory. Compared with previous research results, this research considered
 240 the impact of vehicle driving speed on emissions and the differences in emissions between holiday,
 241 workday, and weekend, and its estimated emissions in this study fell within the ranges of other estimation
 242 results (Table 1).



243
 244 **Figure 3. Geospatial distribution of passenger vehicle emissions and the disparities between urban and rural**
 245 **areas: (a) total pollution-eq emissions (TPEs) at $0.01^\circ \times 0.01^\circ$ resolution and (b) urban-rural differences in**
 246 **vehicle emission densities in four major urban agglomerations (BTH: the Beijing-Tianjin-Hebei region; YRD:**
 247 **the Yangtze River Delta region; PRD: the Pearl River Delta region; SCB: the Sichuan Basin) in 2019.**

248 **Table 1 Comparison and validation with previous studies. (Unit: ten thousand tons)**

References	Year	CO	VOCs	NO _x	NH ₃	PM
This study	2019	408.78	106.94	21.17	7.75	0.195
Liu H et al.(2017)	2015	—	67.4	—	—	—
Li S et al.(2020a)	2017	—	—	—	7.5	—
Li S et al.(2023a)	2019	430	95	26.75	8.9	0.17
MEE(2020a)	2019	456.4	121	25	—	0.1
Qi Z et al.(2023)	2019	625	126	27.5	—	0.21

249 3.3. Temporal variation of passenger vehicle emissions

250 3.3.1 Seasonal and daily variation

251 Analysis of passenger vehicle emissions revealed distinct seasonal patterns across different regions
 252 (Fig.4c). Specifically, the PRD experienced higher emissions in summer, while the YRD, BTH, and SCB



regions had higher emissions in winter (Fig. 4c) (Shao et al., 2009; Jiang et al., 2020; Sun et al., 2022). This high winter emission pattern was primarily attributed to adverse weather conditions, which induced prolonged vehicle idling, and reduced driving speeds (Lu et al., 2019). Moreover, vehicles often needed to turn on additional heating equipment, which increased engine load and consequently affected emissions (Abediasl et al., 2023). Notably, Guangdong recorded the highest emissions (Fig. 4a), due to its subtropical climate with approximately 80% relative humidity (Liu et al., 2020) and had a high volume of traffic (Yang et al., 2022; Krotkov et al., 2016).

This study considered the impact of workday, weekend, and holiday on daily emissions. During the Spring Festival and National Day, people opted for public transportation for long-distance travel or returning home at the holiday's onset, resulting in the lowest passenger vehicle emissions on the first day, gradually increasing in the following days (Fig. 4b) (Zhang and Gao, 2023b). Passenger vehicle emissions normally exhibited a notable weekend effect, with reduced levels on weekend relative to workday (Fig. S3), and daily average pollutant emissions on holiday were 0.92 times those of workday (Wu et al., 2022; Tong et al., 2020). Specifically at daily emissions, for example, from June 17 to June 22, the BTH, YRD, PRD, and SCB regions exhibited notable differences in emission variations. The YRD and PRD regions experienced emission peaks on Friday, while the BTH reached its highest emission level on Monday, corroborating the findings of Wu et al. (Wu et al., 2022) and Zheng et al. (Zheng et al., 2009).

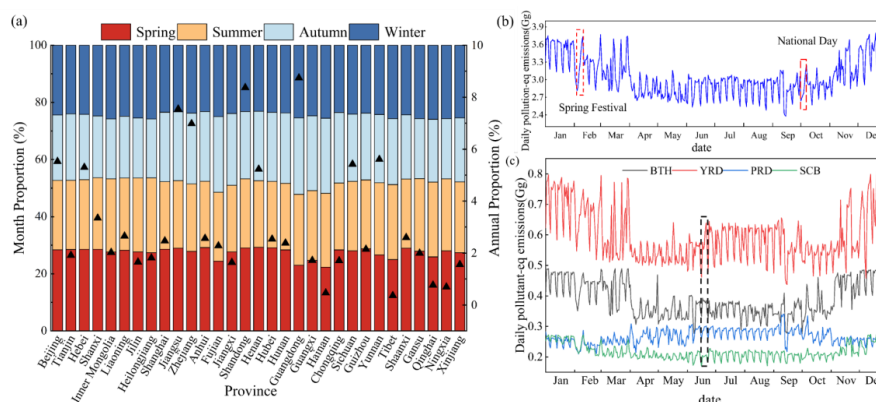


Figure 4. Seasonal and daily scale variations in pollutant emissions: (a) TPEs by province in different months; (b) Daily changes in TPEs across the country and (c) in four major urban agglomerations (BTH, YRD, PRD, SCB).



3.3.2 Hourly variation

The hourly average TPEs varied among workday, weekend, and holiday (Fig.5a). Peak emission periods were mainly concentrated between 8:00 and 9:00 in the morning and between 16:00 and 17:00 in the afternoon, similar to the daily variation trend of traffic volume (Yang et al., 2019; Shang et al., 2024). During the morning peak, hourly average emissions on workday exceeded those on weekend and holiday by 8% and 5%, respectively, increasing to 12% and 18% during the evening peak. As most private and commercial activities occurred during daylight hours, daytime emissions on workday, weekend, and holiday constituted 85.2%, 84%, and 83.1% of the total daily emissions, respectively.

A distinct variation in the trend of hourly average TPE density is observed across different regions (Fig.5b). The BTH region was highest, followed by the YRD, PRD, and SCB regions. This trend might be related to factors such as traffic conditions, population density, and meteorological conditions in each region (Xie et al., 2019; Yang et al., 2025). The data revealed that the daily average emission densities in the BTH and the YRD were 4.9 times and 4.6 times that of the SCB, respectively. Especially during the peak period at 8:00 in the morning, the hourly average emission densities ratios reached as high as 5.4 times and 5.3 times (Fig.5b). This significant emission difference emphasized the necessity of prioritizing traffic management measures in the BTH region.

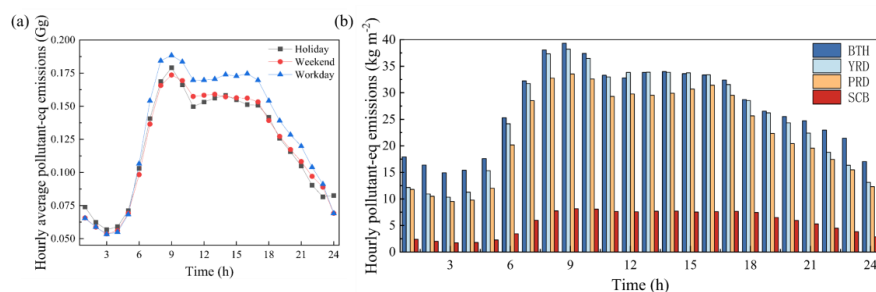


Figure 5. Hourly emission changes for three-day types and regions: (a) hourly total pollutant emission characteristics for weekend, workday and holiday and (b) in four major urban agglomerations (BTH, YRD, PRD, SCB).

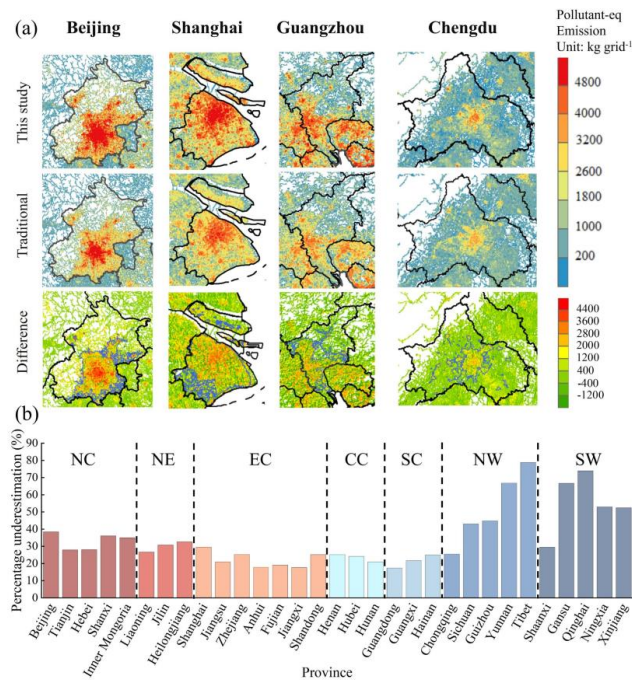
3.4. Comparison of passenger vehicle emissions with conventional algorithms

To improve estimation accuracy, this study obtained gridded speed-corrected emission results based on real-time vehicle driving data and compared them with passenger vehicle emission data obtained using traditional methods.

The improved methodology reflected a more accurate and detailed characterization of passenger



300 vehicle emissions, which were primarily concentrated in urban centers, with emission intensity gradually
301 decreasing from the city center outwards (Fig.6a) (Jing et al., 2016). Compared to those assumed under
302 steady-state driving conditions in the traditional estimation method, real driving patterns, which might
303 involve more frequent acceleration and deceleration, resulted in higher emissions(Zhang et al., 2023a;
304 Wen et al., 2020). This disparity highlighted the limitations of the traditional algorithm, which
305 underestimated emissions on urban center roads while overestimating emissions on some rural roads
306 outside urban centers (Fig.6a). Overall, the estimation using the traditional method underestimated the
307 total emissions by 31.5%, with Sichuan, Beijing, Shanghai, and Guangdong being underestimated by
308 43.1%, 38.4%, 29.6%, and 17.4%, respectively. In Tibet, the average vehicle speed stabilized at around
309 42.5 km h⁻¹, and the SCC analysis revealed a speed correction factor 2.09 times that of the traditional
310 speed correction factor (SCF), leading to the most serious underestimation in this region (Fig.6b)(Sun et
311 al., 2020).



312
313 **Figure 6. Comparison of this study with traditional algorithms: (a) Beijing, Shanghai, Guangzhou to compare**
314 **it with the results of the present study (Difference = This Study — Traditional); (b) The percentage of**
315 **underestimation for each province calculated with the traditional method.**
316 *** The purple boundary is the Urban Growth Boundary (UGB).**



3.5. Model validation

The simulation results of the inventories reflected the temporal variation of pollutant concentrations well. The improved inventory were more consistent with the observed data from the perspective of hourly change ($PM_{2.5}$: $R^2 = 0.850$, NMB = -27.4%; O_3 : $R^2 = 0.771$, NMB = -32.5%) (Fig.7 and Fig.S6). The bias might be caused by the underestimation of the input anthropogenic emission inventory, and it fell within an acceptable and reasonable range verified by comparison with other literature (Ma et al., 2018; Wang et al., 2020 and Georgiou et al., 2022). This result indicated that the accuracy of the emission inventory refined through detailed vehicle speed correction was superior to that constructed by traditional algorithms.

The inventory optimization effect was relatively notable in heavily polluted traffic-intensive areas (Fig.S2b), with an overall 0.36% improvement in NMB ($PM_{2.5}$) and 0.02 improvement in R^2 (O_3). This effect is attributable to the complex characteristics of speed fluctuations in these areas. Specifically, the NMB of $PM_{2.5}$ at the Administrative Center Monitoring Station and Putuo Monitoring Station increased by 0.7% and 0.45%, respectively. Meanwhile, the R^2 of O_3 at the Pudong Chuansha Monitoring Station and Xinghu Garden Monitoring Station rose by 0.05 and 0.04, respectively (Fig.S7). However, this study merely achieved a slight improvement, which may be attributed to the small proportion of emissions from passenger vehicles(e.g., approximately 3.2% for CO, 4.7% for VOC, and 1.2% for NO_x)(Li et al., 2023a). The performance of its simulations would be significantly enhanced when the accuracy of vehicle speed correction for the entire traffic source could be further improved.

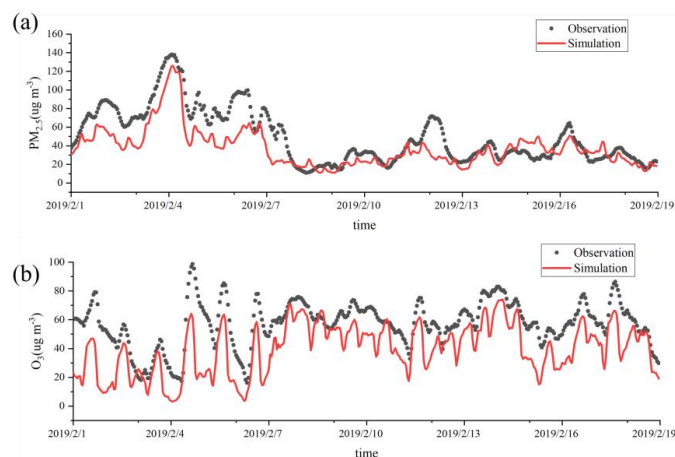


Figure 7. Comparison of temporal variations between simulated results from the improved inventory and



338 **observed data.(a) PM_{2.5}; (b) O₃.**

339 **4. Conclusions**

340 With the rapid growth of the global automobile industry, the proliferation of passenger vehicles has
 341 exacerbated the air pollution problem. Current research lacks a nationwide hourly-scale emissions study
 342 for passenger vehicles. Therefore, this study introduces an innovative approach by utilizing big data of
 343 ride-hailing services and traffic flow models to obtain nationwide hourly gridded speed and traffic
 344 volume, which facilitated the derivation of refined speed correction factors based on actual nationwide
 345 driving behavior at both spatial and temporal scales, enabling the construction of a high-resolution (0.01°
 346 × 0.01°; 1h) emission inventory for passenger vehicle atmospheric pollutants in China. Our emission
 347 inventory revealed that passenger vehicles in China emitted approximately 4087.8, 1069.4, 211.7, 1.9,
 348 and 77.5 kt of CO, VOCs, NO_x, PM, and NH₃, respectively, in 2019.

349 This research showed significant spatial heterogeneity in passenger vehicle emissions in China.
 350 Despite occupying merely 0.8% of the national territory, urban areas generated 35.3% of the country's
 351 total vehicle emissions. High-pollution areas were predominantly concentrated in four major urban
 352 agglomerations (BTH, YRD, PRD, SCB), which contributed significantly to the total emissions at
 353 48.54%, due to high local traffic volumes and relatively low vehicle speeds. Emission density analysis
 354 revealed a hierarchical pattern among urban agglomerations, with the BTH region exhibiting the highest
 355 density, followed by the YRD, PRD, and SCB regions. And the urban emission density of vehicles within
 356 four urban agglomerations was significantly higher compared to rural areas.

357 Passenger vehicle emissions also exhibit multiscale temporal variations. Higher emissions observed
 358 in winter due to weather and driving conditions. In addition, vehicle emissions normally exhibited a
 359 notable weekend effect, with reduced levels on weekend relative to workday, and daily average pollutant
 360 emissions on holiday were 0.92 times those of workday. There are also differences in the hourly average
 361 pollutant emissions across the above three-day types. During the morning peak, hourly average emissions
 362 on workday exceeded those on weekend and holiday by 8% and 5%, respectively, increasing to 12% and
 363 18% during the evening peak. Compared with traditional algorithms, this study could more accurately
 364 identify the actual emission status of urban roads, reducing the deviation in emission estimation. Current
 365 traditional methodology might underestimate by 31.5 %, which is more serious in areas with very little
 366 speed variation. The simulated results for PM_{2.5} and O₃ in this study inventory exhibited good



367 performance.

368 Our study has limitations in the simulation: the ABaCAS database was adopted herein, as it
 369 provides the specific proportion of passenger vehicle emissions. However, compared with the MEIC
 370 anthropogenic emission inventory, the NO_x and VOCs emissions estimated by this database are
 371 underestimated by approximately 20%, which will affect the simulation results to a certain extent.
 372 This consequently might results in the underestimation of the simulation results.

373 Overall, the analytical framework developed in this study accurately quantifies emissions of key
 374 atmospheric pollutants from China's passenger vehicle sector. Although the rapid development of vehicle
 375 electrification and rail transit is driving a gradual reduction in passenger vehicle emissions, passenger
 376 vehicles remain one of the critical sources of pollutants in the transportation sector at the current stage.
 377 The “speed-emission” coupling method validated in this study can be extended to transportation sub-
 378 sectors such as freight trucks and urban public transport, which effectively improves the accuracy of
 379 emission quantification in these fields. To enhance the precision and applicability of our research, more
 380 comprehensive big data will be obtained to provide support for the quality of emission inventories. The
 381 findings also provide an important scientific basis for intelligent transportation and the formulation of
 382 more refined control policies and offer a methodological reference for precise emission management in
 383 the transportation sector through its high-resolution data approach.

384 **Associated content**

385 **Supporting Information**

386 Figures showing distribution of passenger car ownership; weekly change in emission equivalents; spatial
 387 distribution of passenger car emissions for a given three-day period; spatial distribution under
 388 conventional algorithms; comparison of simulated values and observed values of some stations and tables
 389 showing emission factors for each emission standard; sample data for ride-hailing big data; speed
 390 correction curves; deterioration, sulfur correction factors; provincial emissions from passenger cars;
 391 parameter settings and verification results of the model simulation.

392 **Acknowledgments**

393 This work was supported by the National Natural Science Foundation of China (42377393), Jiangsu
 394 Provincial Young Science and Technology Talents Support Project and Postgraduate Research &
 395 Practice Innovation Program of Jiangsu Province(KYCX25_1677).



396 **Author contributions**

397 BL and ZS conceived the study and wrote the paper; BL, ZS, YL, YZ processed the data required for
 398 emission estimation and analyzes the processing results; WG, JL, YY, WZ, ZM optimized the research
 399 methodology and collected relevant data; HL reviewed the manuscript.

400 **Data availability**

401 For the data used in this work, statements have been included about which data are publically available
 402 (accessed through references and links).

403 **Competing interests**

404 The authors declare that they have no conflict of interest.

405 **References**

- 406 Abediasl, H., Balazadeh Meresht, N., Alizadeh, H., Shahbakhti, M., Koch, C. R., and Hosseini, V.: Road
 407 transportation emissions and energy consumption in cold climate cities, *Urban Clim.*, 52,
 408 doi:10.1016/j.uclim.2023.101697, 2023.
- 409 Akash, B., Vikas, S., Leeza, M., Geetam, T., Khaiwal, R., and Suman, M.: Spatially resolved hourly
 410 traffic emission over megacity Delhi using advanced traffic flow data, *Earth Syst. Sci. Data.*, 1-37,
 411 doi:10.5281/zenodo.6553770, 2022.
- 412 Andrew, J. K., Robert, A. H., Gary, A. Kendall.: Effects of Vehicle Speed and Engine Load on Motor
 413 Vehicle Emissions, *Environ. Sci. Technol.*, 37, 3739–3746, doi:10.1021/es0263588 2003.
- 414 Anenberg, S. C., Miller, J., Minjares, R., Du, L., Henze, D. K., Lacey, F., Malley, C. S., Emberson, L.,
 415 Franco, V., Klimont, Z., and Heyes, C.: Impacts and mitigation of excess diesel-related NO_x emissions
 416 in 11 major vehicle markets, *Nature*, 545, 467-471, doi:10.1038/nature22086, 2017.
- 417 Charis, K., Dimitrios, G., Ntziachristos, I. K. L., Pastorello, C., and Dilara, P.: Uncertainty estimates and
 418 guidance for road transport emission calculations., Publications Office of the European Union, EUR,
 419 doi:10.2788/78236, 2010.
- 420 Deng, F., Lv, Z., Qi, L., Wang, X., Shi, M., and Liu, H.: A big data approach to improving the vehicle
 421 emission inventory in China, *Nat. Commun.*, 11, 2801, doi:10.1038/s41467-020-16579-w, 2020.
- 422 Dias, D., Amorim, J. H., Sá, E., Borrego, C., Fontes, T., Fernandes, P., Pereira, S. R., Bandeira, J., Coelho,
 423 M. C., and Tchepel, O.: Assessing the importance of transportation activity data for urban emission
 424 inventories, *Transport. Res. D-tr. E.*, 62, 27-35, doi:10.1016/j.trd.2018.01.027, 2018.
- 425 China Mobile Source Environmental Management Annual Report, Ministry of Ecology and Environment
 426 of the People's Republic of China, 2020a.
- 427 China Statistical Yearbook, NBS (National Bureau of Statistics of China), China Statistics Press, Beijing,
 428 2020b.
- 429 EMEP/EEA air pollutant emission inventory guidebook 2019 : technical guidance to prepare national
 430 emission inventories., European Environment Agency, 2019.
- 431 Environmental Protection Tax Law of the People's Republic of China., MEE (Ministry of Ecology and
 432 Environment), 2018.



- 433 Gao, C., Gao, C., Song, K., Xing, Y., and Chen, W.: Vehicle emissions inventory in high spatial–temporal
 434 resolution and emission reduction strategy in Harbin-Changchun Megalopolis, *Process Saf. Environ.*,
 435 138, 236–245, doi:10.1016/j.psep.2020.03.027, 2020.
- 436 Georgiou, G. K., Christoudias, T., Proestos, Y., Kushta, J., Pikridas, M., Sciare, J., Savvides, C., and
 437 Lelieveld, J.: Evaluation of WRF-Chem model (v3.9.1.1) real-time air quality forecasts over the Eastern
 438 Mediterranean, *Geosci. Model Dev.*, 15, 4129–4146, doi:10.5194/gmd-15-4129-2022, 2022.
- 439 Gómez, C. D., González, C. M., Osses, M., and Aristizábal, B. H.: Spatial and temporal disaggregation
 440 of the on-road vehicle emission inventory in a medium-sized Andean city. Comparison of GIS-based top-
 441 down methodologies, *Atmos. Environ.*, 179, 142–155, doi:10.1016/j.atmosenv.2018.01.049, 2018.
- 442 Guan, D., Ren, N., Wang, K., Wang, Q., and Zhang, H.: Checkpoint data-driven GCN-GRU vehicle
 443 trajectory and traffic flow prediction, *Sci. Rep.*, 14, 30409, doi:10.1038/s41598-024-80563-3, 2024.
- 444 Guo, D., Zhao, J., Xu, Y., Sun, F., Li, K., Wang, J., and Sun, Y.: The Impact of Driving Conditions on
 445 Light-Duty Vehicle Emissions in Real-World Driving, *Transport*, 35, 379–388,
 446 doi:10.3846/transport.2020.12168, 2020.
- 447 Hou, G., Chen, S., and Chen, F.: Framework of simulation-based vehicle safety performance assessment
 448 of highway system under hazardous driving conditions, *Transport. Res. C-Em.*, 105, 23–26,
 449 doi:10.1016/j.trc.2019.05.035, 2019.
- 450 Huo, H., Zhang, Q., He, K., Wang, Q., Yao, Z., and Street, D. G.: High-Resolution Vehicular Emission
 451 Inventory Using a Link-Based Method: A Case Study of Light-Duty Vehicles in Beijing, *Environ. Sci.*
 452 *Technol.* 43, 7, 2394–2399, doi:10.1021/es802757a, 2009.
- 453 Jiang, P., Zhong, X., and Li, L.: On-road vehicle emission inventory and its spatio-temporal variations in
 454 North China Plain, *Environ. Pollut.*, 267, 115639, doi:10.1016/j.envpol.2020.115639, 2020.
- 455 Jing, B., Wu, L., Mao, H., Gong, S., He, J., Zou, C., Song, G., Li, X., and Wu, Z.: Development of a
 456 vehicle emission inventory with high temporal–spatial resolution based on NRT traffic data and its impact
 457 on air pollution in Beijing – Part 1: Development and evaluation of vehicle emission inventory, *Atmos.*
 458 *Chem. Phys.*, 16, 3161–3170, doi:10.5194/acp-16-3161-2016, 2016.
- 459 Jinping, W., Haixia, F., Huanhuan, Z., Guohua, H., Miaomiao, H., Qingli, S., and Er-wei, N.: A temporal
 460 allocation method of motor vehicle emission inventories, *J. Automot. Saf. Energy.*, 15, 387–394,
 461 doi:10.3969/j.issn.1674-8484.2024.03.012, 2024.
- 462 Krotkov, N. A., McLinden, C. A., Li, C., Lamsal, L. N., Celarier, E. A., Marchenko, S. V., Swartz, W. H.,
 463 Bucsela, E. J., Joiner, J., Duncan, B. N., Boersma, K. F., Veefkind, J. P., Levelt, P. F., Fioletov, V. E.,
 464 Dickerson, R. R., He, H., Lu, Z., and Streets, D. G.: Aura OMI observations of regional SO₂ and NO₂
 465 pollution changes from 2005 to 2015., *Atmos. Chem. Phys.*, 16, 4605–4629, doi:10.5194/acpd-15-26555-
 466 2015, 2016.
- 467 Li, S., Lang, J., Zhou, Y., Liang, X., Chen, D., and Wei, P.: Trends in ammonia emissions from light-duty
 468 gasoline vehicles in China, 1999–2017, *Sci. Total Environ.*, 700, 134359,
 469 doi:10.1016/j.scitotenv.2019.134359, 2020a.
- 470 Li, S., Wang, S., Wu, Q., Zhang, Y., Ouyang, D., Zheng, H., Han, L., Qiu, X., Wen, Y., Liu, M., Jiang, Y.,
 471 Yin, D., Liu, K., Zhao, B., Zhang, S., Wu, Y., and Hao, J.: Emission trends of air pollutants and CO₂ in
 472 China from 2005 to 2021, *Earth Syst. Sci. Data.*, 15, 2279–2294, doi:10.5194/essd-15-2279-2023, 2023a.
- 473 Li, Y., Lv, C., Yang, N., Liu, H., and Liu, Z.: A study of high temporal-spatial resolution greenhouse gas
 474 emissions inventory for on-road vehicles based on traffic speed-flow model: A case of Beijing, *J. Clean.*
 475 *Prod.*, 277, doi:10.1016/j.jclepro.2020.122419, 2020b.
- 476 Li, Y., Li, B., Liao, H., Zhou, B. B., Wei, J., Wang, Y., Zang, Y., Yang, Y., Liu, R., and Wang, X.: Changes



in PM_{2.5}-related health burden in China's poverty and non-poverty areas during 2000-2020: A health inequality perspective, *Sci. Total Environ.*, 861, 160517, doi:10.1016/j.scitotenv.2022.160517, 2023b.

Liu, H., Man, H., Cui, H., Wang, Y., Deng, F., Wang, Y., Yang, X., Xiao, Q., Zhang, Q., Ding, Y., and He, K.: An updated emission inventory of vehicular VOCs and IVOCs in China, *Atmos. Chem. Phys.*, 17, 12709-12724, doi:10.5194/acp-17-12709-2017, 2017.

Liu, Y. H., Ma, J. L., Li, L., Lin, X. F., Xu, W. J., and Ding, H.: A high temporal-spatial vehicle emission inventory based on detailed hourly traffic data in a medium-sized city of China, *Environ. Pollut.*, 236, 324-333, doi:10.1016/j.envpol.2018.01.068, 2018.

Liu, Z., Yang, H., and Wei, X.: Spatiotemporal Variation in Relative Humidity in Guangdong, China, from 1959 to 2017, *Water*, 12, doi:10.3390/w12123576, 2020.

Loder, A., Ambuhl, L., Menendez, M., and Axhausen, K. W.: Understanding traffic capacity of urban networks, *Sci. Rep.*, 9, 16283, doi:10.1038/s41598-019-51539-5, 2019.

Lu, Z., Kwon, T. J., and Fu, L.: Effects of winter weather on traffic operations and optimization of signalized intersections, *Journal of Traffic and Transportation Engineering (English Edition)*, 6, 196-208, doi:10.1016/j.jtte.2018.02.002, 2019.

Luo, Z., Wang, Y., Lv, Z., He, T., Zhao, J., Wang, Y., Gao, F., Zhang, Z., and Liu, H.: Impacts of vehicle emission on air quality and human health in China, *Sci. Total Environ.*, 813, 152655, doi:10.1016/j.scitotenv.2021.152655, 2022.

Ma, D., Wu, X., Sun, X., Zhang, S., Yin, H., Ding, Y., and Wu, Y.: The Characteristics of Light-Duty Passenger Vehicle Mileage and Impact Analysis in China from a Big Data Perspective, *Atmosphere*, 13, doi:10.3390/atmos13121984, 2022.

Ma, X.Y., Sha, T., Wang, J.Y., Jia, H.L., Tian, R.: Investigating impact of emission inventories on PM_{2.5} simulations over North China Plain by WRF-Chem. *Atmos. Environ.*, 195, 125-140, doi:10.1016/j.atmosenv.2018.09.058, 2018.

Qi, Z., Zheng, Y., Feng, Y., Chen, C., Lei, Y., Xue, W., Xu, Y., Liu, Z., Ni, X., Zhang, Q., Yan, G., and Wang, J.: Co-drivers of Air Pollutant and CO₂ Emissions from On-Road Transportation in China 2010-2020, *Environ. Sci. Technol.*, 57, 20992-21004, doi:10.1021/acs.est.3c08035, 2023.

Shang, W.-L., Song, X., Chen, Y., Yang, X., Liang, L., Deveci, M., Cao, M., Xiang, Q., and Yu, Q.: Congestion and Pollutant Emission Analysis of Urban Road Networks Based on Floating Vehicle Data, *Urban. Clim.*, 53, doi:10.1016/j.uclim.2023.101794, 2024.

Shao, M., Zhang, Y., Zeng, L., Tang, X., Zhang, J., Zhong, L., and Wang, B.: Ground-level ozone in the Pearl River Delta and the roles of VOC and NO_x in its production, *J. Environ. Manage.*, 90, 512-518, doi:10.1016/j.jenvman.2007.12.008, 2009.

Sun, J., Qin, M., Xie, X., Fu, W., Qin, Y., Sheng, L., Li, L., Li, J., Sulaymon, I. D., Jiang, L., Huang, L., Yu, X., and Hu, J.: Seasonal modeling analysis of nitrate formation pathways in Yangtze River Delta region, China, *Atmos. Chem. Phys.*, 22, 12629-12646, doi:10.5194/acp-22-12629-2022, 2022.

Sun, S., Sun, L., Liu, G., Zou, C., Wang, Y., Wu, L., and Mao, H.: Developing a vehicle emission inventory with high temporal-spatial resolution in Tianjin, China, *Sci. Total Environ.*, 776, doi:10.1016/j.scitotenv.2021.145873, 2021.

Sun, S., Jin, J., Xia, M., Liu, Y., Gao, M., Zou, C., Wang, T., Lin, Y., Wu, L., Mao, H., and Wang, P.: Vehicle emissions in a middle-sized city of China: Current status and future trends, *Environ. Int.*, 137, 105514, doi:10.1016/j.envint.2020.105514, 2020.

The Announcement about Releasing Five National Technical Guidelines of the Air Pollutant Emissions Inventory., MEE (Ministry of Ecology and Environment), 2014.



- 521 Tong, R., Liu, J., Wang, W., and Fang, Y.: Health effects of PM_{2.5} emissions from on-road vehicles during
522 weekdays and weekends in Beijing, China, *Atmos. Environ.*, 223, doi:10.1016/j.atmosenv.2019.117258,
523 2020.
- 524 Wang, P., Qiao, X., Zhang, H. L.: Modeling PM_{2.5} and O₃ with aerosol feedbacks using WRF/Chem over
525 the Sichuan Basin, southwestern China. *Chemosphere*, 254,
526 126735, doi:10.1016/j.chemosphere.2020.126735, 2020.
- 527 Wen, Y., Liu, M., Zhang, S., Wu, X., Wu, Y., and Hao, J.: Updating On-Road Vehicle Emissions for China:
528 Spatial Patterns, Temporal Trends, and Mitigation Drivers, *Environ. Sci. Technol.*, 57, 14299-14309,
529 doi:10.1021/acs.est.3c04909, 2023.
- 530 Wen, Y., Zhang, S., Zhang, J., Bao, S., Wu, X., Yang, D., and Wu, Y.: Mapping dynamic road emissions
531 for a megacity by using open-access traffic congestion index data, *Appl. Energ.*, 260,
532 doi:10.1016/j.apenergy.2019.114357, 2020.
- 533 Wen, Y., Wu, R., Zhou, Z., Zhang, S., Yang, S., Wallington, T. J., Shen, W., Tan, Q., Deng, Y., and Wu,
534 Y.: A data-driven method of traffic emissions mapping with land use random forest models, *Appl. Energ.*,
535 305, doi:10.1016/j.apenergy.2021.117916, 2022.
- 536 Wu, L., Xie, J., and Kang, K.: Changing weekend effects of air pollutants in Beijing under 2020 COVID-
537 19 lockdown controls, *npj Urban Sustainability*, 2, 23, doi:10.1038/s42949-022-00070-0, 2022.
- 538 Xie, R., Wei, D., Han, F., Lu, Y., Fang, J., Liu, Y., and Wang, J.: The effect of traffic density on smog
539 pollution: Evidence from Chinese cities, *Technol. Forecast. Soc.*, 144, 421-427,
540 doi:10.1016/j.techfore.2018.04.023, 2019.
- 541 Xu, X., Tan, M., Liu, X., Wang, X., and Xin, L.: Stability and Changes in the Spatial Distribution of
542 China's Population in the Past 30 Years Based on Census Data Spatialization, *Remote Sensing*, 15,
543 doi:10.3390/rs15061674, 2023.
- 544 Xu, Y., Liu, Z., Xue, W., Yan, G., Shi, X., Zhao, D., Zhang, Y., Lei, Y., and Wang, J.: Identification of on-
545 road vehicle CO₂ emission pattern in China: A study based on a high-resolution emission inventory,
546 *Resour. Conserv. Recy.*, 175, doi:10.1016/j.resconrec.2021.105891, 2021.
- 547 Yang, D., Zhang, S., Niu, T., Wang, Y., Xu, H., Zhang, K. M., and Wu, Y.: High-resolution mapping of
548 vehicle emissions of atmospheric pollutants based on large-scale, real-world traffic datasets, *Atmos.*
549 *Chem. Phys.*, 19, 8831-8843, doi:10.5194/acp-19-8831-2019, 2019.
- 550 Yang, L., Wu, D., Cao, S., Zhang, W., Zheng, Z., and Liu, L.: Transportation Interrelation Embedded in
551 Regional Development: The Characteristics and Drivers of Road Transportation Interrelation in
552 Guangdong Province, China, *Sustainability*, 14, doi:10.3390/su14105925, 2022.
- 553 Yang, S., Wu, J., Qi, G., and Tian, K.: Analysis of traffic state variation patterns for urban road network
554 based on spectral clustering, *Adv. Mech. Eng.*, doi:10.1177/1687814017723790, 2017.
- 555 Yang, W., Yu, C., Yuan, W., Wu, X., Zhang, W., and Wang, X.: High-resolution vehicle emission
556 inventory and emission control policy scenario analysis, a case in the Beijing-Tianjin-Hebei (BTH)
557 region, China, *J. Clean. Prod.*, 203, 530-539, doi:10.1016/j.jclepro.2018.08.256, 2018.
- 558 Yang, X., Wang, Q., Liu, L., Tian, J., Xie, H., Wang, L., Cao, Y., and Ho, S. S. H.: Impacts of emission
559 reduction and meteorological conditions on air quality improvement from 2016 to 2020 in the Northeast
560 Plain, China, *J. Environ. Sci.*, 151, 484-496, doi:10.1016/j.jes.2024.04.017, 2025.
- 561 Yu, K. A., McDonald, B. C., and Harley, R. A.: Evaluation of Nitrogen Oxide Emission Inventories and
562 Trends for On-Road Gasoline and Diesel Vehicles, *Environ. Sci. Technol.*, 55, 6655-6664,
563 doi:10.1021/acs.est.1c00586, 2021.
- 564 Zhang, J., Peng, J., Song, A., Lv, Z., Tong, H., Du, Z., Guo, J., Wu, L., Wang, T., Hallquist, M., and Mao,



565 H.: Marked impacts of transient conditions on potential secondary organic aerosol production during
 566 rapid oxidation of gasoline exhausts, *npj Clim. Atmos. Sci.* 6, doi:10.1038/s41612-023-00385-4, 2023a.
 567 Zhang, X. and Gao, J.: The analysis and solution for intercity travel behaviors during holidays in the
 568 post-epidemic era based on big data, *PLoS One*, 18, e0288510, doi:10.1371/journal.pone.0288510,
 569 2023b.
 570 Zheng, B., Huo, H., Zhang, Q., Yao, Z. L., Wang, X. T., Yang, X. F., Liu, H., and He, K. B.: High-
 571 resolution mapping of vehicle emissions in China in 2008, *Atmos. Chem. Phys.*, 14, 9787-9805,
 572 doi:10.5194/acp-14-9787-2014, 2014.
 573 Zheng, J., Zhang, L., Che, W., Zheng, Z., and Yin, S.: A highly resolved temporal and spatial air pollutant
 574 emission inventory for the Pearl River Delta region, China and its uncertainty assessment, *Atmos.*
 575 *Environ.*, 43, 5112-5122, doi:10.1016/j.atmosenv.2009.04.060, 2009.
 576 Gu, Z., Duan, X., Liu, B., Hu, J., and He, J.: The spatial distribution and temporal variation of rainfall
 577 erosivity in the Yunnan Plateau, Southwest China: 1960–2012, *Catena*, 145, 291-300,
 578 doi:10.1016/j.catena.2016.06.028, 2016.
 579 Zhou, Y., Zhao, Y., Mao, P., Zhang, Q., Zhang, J., Qiu, L., and Yang, Y.: Development of a high-resolution
 580 emission inventory and its evaluation through air quality modeling for Jiangsu Province, China, *Atmos.*
 581 *Chem. Phys.*, 17, 211–233, doi:10.5194/acp-2016-567, 2016.
 582